American Mineralogist, Volume 92, pages 1080–1086, 2007

TEM investigation of Ca-rich plagioclase: Structural fluctuations related to the $I\bar{1}$-$P\bar{1}$ phase transition

Péter Németh,[1,2] Mario Tribaudino,[3] Emiliano Bruno,[4] and Peter R. Buseck[1,2,*]

[1]School of Earth and Space Exploration, Arizona State University, Tempe, Arizona 85287-1404, U.S.A.
[2]Department of Chemistry and Biochemistry, Arizona State University, Tempe, Arizona 85287-1604, U.S.A.
[3]Dipartimento di Scienze della Terra, Università di Parma, Parco Area delle Scienze 157/A, Parma, 43100, Italy
[4]Dipartimento di Scienze Mineralogiche e Petrologiche, Università di Torino, Via Valperga Caluso 35, Torino, 10125, Italy

Abstract

We used transmission electron microscopy (TEM) to understand microstructural changes accompanying the reversible $I\bar{1}$-$P\bar{1}$ phase transition in Ca-rich plagioclase as a function of Na content. The transition produces *c*- and *d*-type domains that have $P\bar{1}$ symmetries, and the symmetries of domain walls are $I\bar{1}$. Based on diffractograms and contrast differences of high-resolution TEM (HRTEM) images, we infer that structural differences occur on a scale of tens of nanometers, giving rise to structural fluctuations. These variations can be followed on a nanometer scale using HRTEM images. We propose a model with a body-centered Al-Si framework and single Ca sites for the $I\bar{1}$ domains. The $P\bar{1}$ domains of anorthite with high Al-Si ordering are homogeneous. In contrast, structural fluctuations occur in both anorthite with lower Al-Si ordering and in Na-bearing plagioclase. The magnitudes of the fluctuations decrease with increases in Na content.

Keywords: $I\bar{1}$-$P\bar{1}$ phase transition, Ca-rich plagioclase, HRTEM, structural fluctuations

Introduction

Plagioclase feldspars are major constituents of Earth's crust. Chemically, they are solid solutions of albite ($NaAlSi_3O_8$) and anorthite ($CaAl_2Si_2O_8$). Structurally, they consist of a framework of AlO_4 and SiO_4 tetrahedra that are linked by shared O atoms. Upon cooling, different Al-Si ordering schemes develop to avoid the energetically unfavorable Al-O-Al linking (Loewenstein 1954; Putnis 1992). The first plagioclase that crystallizes from a melt should evolve during cooling to a two-phase assemblage (e.g., Carpenter 1994). This process is, however, kinetically inhibited, and metastable microstructures form (Smith 1974; Kroll and Ribbe 1980). Such microstructures are of interest because they have the potential of recording cooling histories (e.g., Brown and Parsons 1994; Carpenter 1994).

Albite-rich plagioclase has $C\bar{1}$ symmetry, and calcic plagioclase has $I\bar{1}$ and $P\bar{1}$ symmetries (e.g., Carpenter 1994). Complexities arise through the presence of incommensurate phases for slowly cooled, ordered plagioclase with intermediate Ca contents.

A reversible phase transition from $I\bar{1}$ to $P\bar{1}$ in anorthite, first discovered by Brown et al. (1963), occurs at 514 K (e.g., Ghose et al. 1993). The temperature of the transition decreases with increases in the albite content (Redfern et al. 1988). The symmetry change is related to displacive crumpling of the Al-Si framework and the loss of the body-centering among the Ca atoms. Different $P\bar{1}$ atomic configurations occur depending on the extent of the framework crumpling, and they are revealed by differences in cell parameters (Salje 1987). In this paper, we focus on the $I\bar{1}$-$P\bar{1}$ transition and associated microstructures in Ca-rich plagioclase.

Generally the $I\bar{1}$-$P\bar{1}$ phase transition has been studied by bulk methods such as X-ray diffraction (e.g., Angel et al. 1990; Carpenter et al. 1990) and infrared (IR) spectroscopy (Redfern and Salje 1987; Atkinson et al. 1999). Transmission electron microscopy (TEM) has also been used and revealed the occurrence of $P\bar{1}$ domains and domain boundaries (e.g., McLaren 1973; Czank et al. 1973; Van Tendeloo et al. 1989; Tribaudino et al. 2000). Such domains were considered to be displaced with respect to each other (i.e., antiphase domains), and boundaries were supposed to have $I\bar{1}$ symmetries (e.g., Van Tendeloo et al. 1989; Tribaudino et al. 2000). However, McLaren (1973) pointed out that not all $P\bar{1}$ domains are displaced with respect to each other and that high-resolution TEM (HRTEM) is required to study the walls between $P\bar{1}$ domains. Therefore, here we refer to these features as $P\bar{1}$ domains and domain boundaries. Van Tendeloo et al. (1989) showed the presence of micrometer-sized $P\bar{1}$ domains with sharp interfaces in anorthite. In contrast, McLaren (1973) showed smaller (tens of nanometers) $P\bar{1}$ domains separated by boundaries in plagioclase with $An_{95}Ab_5$ (An: anorthite; Ab: albite) composition. Tribaudino et al. (2000) studied a synthetic anorthite, and they also found small, elongated $P\bar{1}$ domains separated by boundaries.

The $I\bar{1}$-$P\bar{1}$ phase transition is of interest as it couples with Al-Si ordering (Redfern et al. 1988), which is associated with the $C\bar{1}$-$I\bar{1}$ phase transition and related to variations of strain and elastic proper-

* E-mail: pbuseck@asu.edu

0003-004X/07/0007–1080$05.00/DOI: 10.2138/am.2007.2504

ties (e.g., Dove 1997). Differences in the elastic constants arising from the displacive phase transition can cause a wide variety of elastic anomalies (Carpenter and Salje 1998; Carpenter 2006), some of which may be traced in seismic profiles (e.g., Kono et al. 2004).

In the present study, four plagioclase samples with compositions ranging from An_{100} to $An_{85}Ab_{15}$ were investigated using HRTEM imaging. Our goals were to study at room temperature the $P\bar{1}$-$I\bar{1}$ transition induced in anorthite by increases in the Ab content and to detect the symmetry and structural differences on a nanometer scale.

Samples and experimental methods

We investigated a natural and a synthetic anorthite and two Ca-rich plagioclase samples. The natural anorthite (An_{100}) is from the same locality (Val di Fassa, also reported as Val Pasmeda, Italy) as was used by Van Tendeloo et al. (1989) and Angel et al. (1990). The synthetic anorthite (An_{100}) is the same sample as was characterized by Tribaudino et al. (2000). Here we reinvestigated only its HRTEM image (Fig. 6 in Tribaudino et al. 2000). The $An_{92}Ab_8$ and $An_{85}Ab_{15}$ plagioclases are from the Ivrea-Verbano (Italy) mafic complex and a dike of the Traversella (Italy) granodioritic massif, respectively. The natural An_{100} grains are associated with quartz and chlorite. The $An_{92}Ab_8$ sample consists of homogeneous euhedral crystals a few millimeters across, with triple junctions of orthopyroxene and biotite. The grains in the $An_{85}Ab_{15}$ sample occur as zoned phenocrysts embedded in a matrix containing plagioclase crystals with different compositions.

The average compositions of the $An_{92}Ab_8$ and $An_{85}Ab_{15}$ samples were published by Bruno and Facchinelli (1979). The composition of the natural An_{100} sample was determined using a scanning electron microscope (operated in energy dispersive mode at 15 kV and 1.2 nA with beam diameter of 100 nm).

$An_{92}Ab_8$ and $An_{85}Ab_{15}$ crystals suitable for TEM observations were prepared from oriented, polished petrographic thin sections. Three-millimeter discs were removed by coring and then thinned by using a Gatan 691 Precision Ion Polishing System (accelerating voltage = 5 keV, milling angle = 8°). Natural An_{100} grains were crushed under ethanol and deposited onto copper grids covered by lacey-carbon supporting films. TEM data were acquired with a JEOL JEM 4000EX TEM (400 kV; LaB_6 filament, top-entry, double-tilt stage; C_s = 1 mm; point-resolution = 0.17 nm) at Arizona State University. The estimated thicknesses of the investigated TEM foils were about 10 to 20 nm. HRTEM images were simulated with Cerius^2 4.0 software (Molecular Simulation Institute, Inc.) at the microscope experimental conditions (defocus spread = 7 nm, beam divergence = 0.4 mrad). Diffractograms determined from the HRTEM images and intensity profiles were calculated using Gatan Digital Micrograph 2.5.7 software (Meyer et al. 1996). We applied a mask filter using the same software to reduce the background noise and calculate background-filtered images.

Phase transitions and order parameters in plagioclase

The $I\bar{1}$-$P\bar{1}$ phase transition and Q_d

A crystal that experienced the $I\bar{1}$-$P\bar{1}$ phase transition can be recognized by the presence of *c*- and *d*-type domains. They are large in slowly cooled anorthite and small and elongated in rapidly cooled anorthite and in less-calcic plagioclase (Kroll and Ribbe 1980).

The *c*- and *d*-type domains occur in $P\bar{1}$ plagioclase and are revealed in diffraction patterns by *c* ($h + k$ even, l odd) and *d* ($h + k$ odd, l even) reflections, respectively. Such reflections are sharp in Al-Si ordered anorthite, and they are diffuse and elongated in partially Al-Si disordered anorthite and in Na-bearing plagioclase (Carpenter et al. 1985; Carpenter 1991). They are extremely diffuse and elongated in bytownite and almost absent in labradorite.

The $I\bar{1}$-$P\bar{1}$ phase transition can be specified in terms of an order parameter, Q_d, a variable that reflects the extent of the transition and ranges between 0 in the high-symmetry ($I\bar{1}$) phase and 1 at 0 K in the fully transformed, low-symmetry ($P\bar{1}$) phase (Salje 1987). The changes in Q_d as a result of the $I\bar{1}$-$P\bar{1}$ transition are revealed by changes in the intensities of the *c* reflections, the unit-cell parameters (Carpenter et al. 1990), and phonon frequencies and amplitudes shown by IR spectroscopy (Redfern and Salje 1987; Atkinson et al. 1999).

The $C\bar{1}$-$I\bar{1}$ phase transition and Q_{od}

Al-Si ordering in plagioclase associated with the $C\bar{1}$-$I\bar{1}$ phase transition influences the $I\bar{1}$-$P\bar{1}$ transition (Salje 1987). Decreases in Al-Si ordering results in decreases in the spontaneous strain connected with the $I\bar{1}$-$P\bar{1}$ transition and prevents the development of large *c*- and *d*-type domains (Redfern 1992).

A crystal that experienced the $C\bar{1}$-$I\bar{1}$ phase transition can be recognized by the presence of *b*-type domains, and in diffraction patterns *b* ($h + k$ odd, l odd) reflections appear. The order parameter for the $C\bar{1}$-$I\bar{1}$ transition is called Q_{od} (Salje 1987). It varies between 0 for the Al-Si disordered $C\bar{1}$ structure and 1 for the $I\bar{1}$ structure with complete Al-Si ordering.

Results

c and *d* reflections and *c*-type domains

Selected-area electron diffraction (SAED) patterns were obtained for different orientations (Figs. 1a–1c) to determine the presence of *c* and *d* reflections, which are characteristic of $P\bar{1}$ anorthite. The sizes and elongations of the *c*-type domains

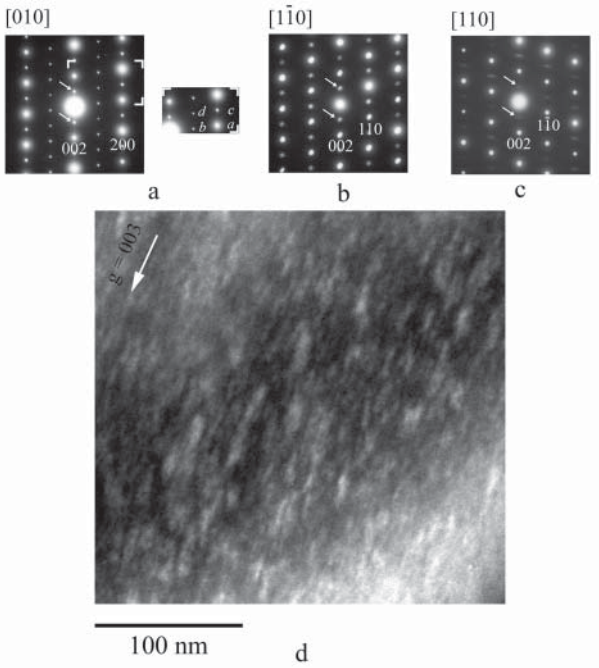

Figure 1. SAED patterns of Ca-rich plagioclase samples and DF image of $An_{92}Ab_8$. (**a**) Natural An_{100}; the insert indicated by white corners shows the letter labels used in the literature for these reflections (Smith 1974). The *a* reflections belong to the plagioclase subcell and are not considered here. (**b**) $An_{92}Ab_8$; (**c**) $An_{85}Ab_{15}$; arrows show *c* reflections ($h + k$ even, l odd); (**d**) DF image of $An_{92}Ab_8$ shows *c*-type domains (light lenses) in a gray matrix. The image is viewed along [1$\bar{1}$0] and taken with a tilt of ~1° from the Bragg condition. The white arrow shows the diffracting vector direction.

were investigated in the $An_{92}Ab_8$ plagioclase in dark-field (DF) images using the *c* reflections.

Sharp *a*, *b*, *c*, and *d* reflections appear in the natural An_{100} sample (Fig. 1a). The *c* reflections are sharp in the $An_{92}Ab_8$ plagioclase when viewed along $[1\bar{1}0]$ (Fig. 1b), but in other orientations they are slightly elongated. The *c* reflections are elongated and diffuse in the $An_{85}Ab_{15}$ sample (Fig. 1c).

The *c*-type domains are large (μm size; e.g., Van Tendeloo et al. 1989) in the natural An_{100} sample, beyond the size of the crushed grains. In $An_{92}Ab_8$ plagioclase the *c*-type domains (Fig. 1d) appear as bright lenses in DF images. The average width of the domains in $An_{92}Ab_8$ plagioclase is about 5 nm. The domain walls between the *c*-type domains are 1-nm wide in Figure 1d. In sample $An_{85}Ab_{15}$, no contrast is apparent in DF imaging of a diffuse *c* reflection.

Symmetry variations on the nanometer scale

Symmetry variations were investigated by using HRTEM images and calculated diffractograms. Areas with $P\bar{1}$ symmetry are apparent in HRTEM images if 00*l* lattice fringes with 1.28-nm periodicity occur and in the corresponding diffractograms if *c* reflections are present. In $I\bar{1}$, 002 fringes with 0.64-nm periodicity occur in HRTEM images, and *c* reflections are absent in the diffractograms. The spacings of plagioclase (001) and (002) planes are 1.28 nm and 0.64 nm, respectively.

The imaged area of the natural An_{100} sample (Fig. 2) has uniform $P\bar{1}$ symmetry, as was also observed for this sample by Van Tendeloo et al. (1989). Fringes with 1.28-nm periodicity are pronounced in the background-filtered image (Fig. 2).

The HRTEM image of $An_{92}Ab_8$ plagioclase looks misleadingly uniform (Fig. 3a). By examining this image at a glancing angle from right to left (or left to right) it can be seen that parts of the figure have predominant 00*l* fringe periodicities of 1.28-nm and other areas have 0.64-nm spacings. These same spacings also occur in the background-filtered image (Fig. 3e). The diffractograms calculated from different regions show $P\bar{1}$ (Fig. 3d) and $I\bar{1}$ (Figs. 3b and 3c) symmetries. Not all $P\bar{1}$ regions are displaced with respect to each other, in agreement with previous findings of McLaren (1973), and a well-defined boundary between the $P\bar{1}$ and $I\bar{1}$ domains cannot be observed. We followed the intensity differences of *c* reflections from place to place within a region of uniform thickness and apparently uniform symmetry (Figs. 3f and 4a). Sharp *c* reflections occur in Figure 4b, and they are streaked and less intense in Figures 4c and 4d, suggesting that structural differences can occur on a scale of tens of nanometers.

In sample $An_{85}Ab_{15}$, only fringes having periodicities of 0.64 nm are apparent in both the experimental HRTEM image (Fig. 5a) and the background-filtered image (Fig. 5c). Sharp *c* reflections are absent in the diffractograms. However, split reflections similar to incommensurate reflections appear in Figure 5b. The orientation of the split reflections is the same as those of the elongated *c* reflections in the SAED pattern (Fig. 1c).

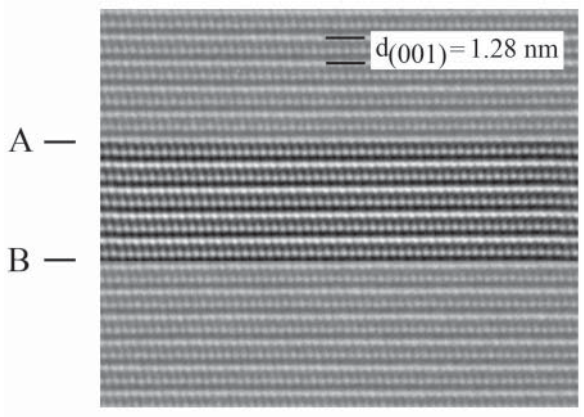

FIGURE 2. HRTEM image of natural An_{100} along [010]. A background-filtered region is inserted between A and B.

DISCUSSION

$I\bar{1}$ anorthite

Anorthite can occur with either $I\bar{1}$ or $P\bar{1}$ symmetry. In $I\bar{1}$, the coordinates of equivalent atom positions are related by 1/2 + x, 1/2 + y, 1/2 + z translations. Each atom in an independent

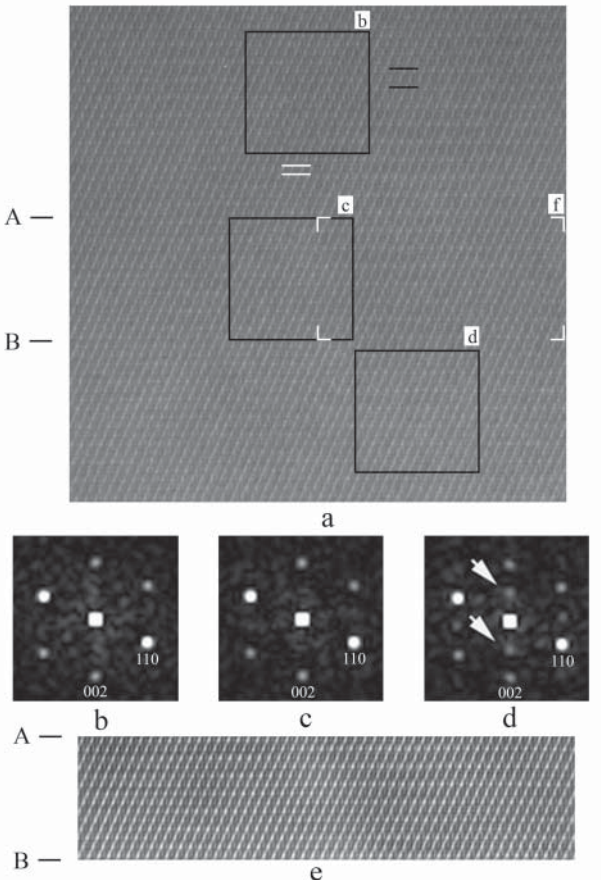

FIGURE 3. HRTEM image of $An_{92}Ab_8$ along $[1\bar{1}0]$ and diffractograms of selected areas. (**a**) HRTEM image. Black and white lines mark 00*l* fringes having 1.28- and 0.64-nm spacings, respectively. (**b**) and (**c**) diffractograms from boxes b and c show a lack of *c* reflections; (**d**) diffractogram from box d shows *c* reflections (white arrows); (**e**) background-filtered image area between A and B. Box f, indicated by white corners, is enlarged in Figure 4.

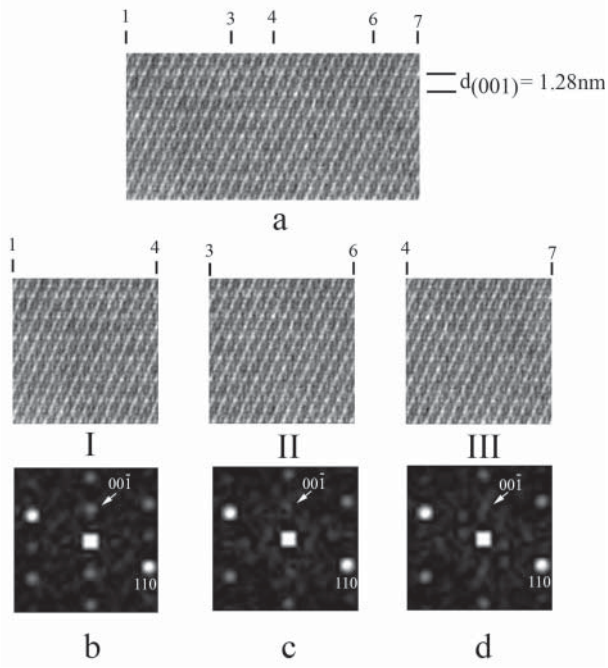

FIGURE 4. Enlarged area of the HRTEM image of $An_{92}Ab_8$ from box f in Figure 3a. (**a**) HRTEM image. Boxes marked I, II, and III are regions corresponding to the numbered lines on the top of **a**. Partial superposition of the boxes is present. Diffractograms (**b**, **c**, and **d**) from boxes I, II, and III, respectively, show the intensity changes of *c* reflections (white arrows) across this small region.

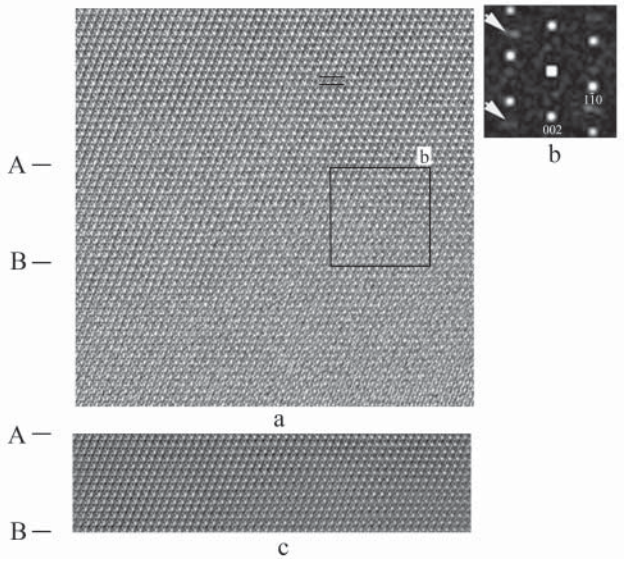

FIGURE 5. HRTEM image of $An_{85}Ab_{15}$ along [110] and a diffractogram. (**a**) HRTEM image. Black lines show (002) fringes with 0.64-nm spacings. (**b**) Calculated diffractogram from box b shows split reflections (white arrows); (**c**) background-filtered image area between A and B.

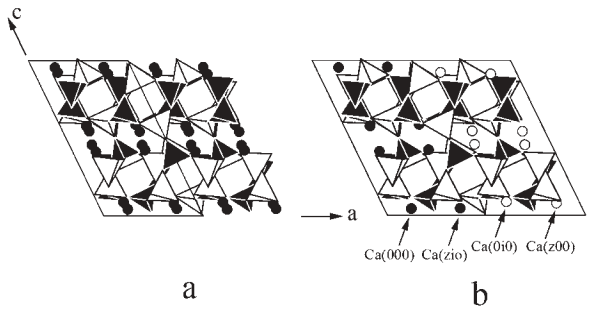

FIGURE 6. Structure models of $I\bar{1}$ anorthite along [010]. (**a**) The model of Angel et al. (1990) shows split Ca sites (black circles). Black lines border a unit cell. (**b**) A model built from two unit cells (doubled *a* dimension) of (**a**) exhibits an ordered (black circles) and an anti-ordered (white circles) Ca configuration (see text). Different Ca sites are marked Ca(000), Ca(zi0), Ca(0i0), and Ca(z00). Black and white polyhedra are SiO_4 and AlO_4 tetrahedra, respectively.

position in $I\bar{1}$ has two atoms in the corresponding $P\bar{1}$ structure. In $P\bar{1}$, there are four independent Ca sites: Ca(000), Ca(0i0), Ca(z00), and Ca(zi0) (Kempster et al. 1962), where i and z denote translations of ~1/2[111] and ~1/2[001] according to the feldspar subcell. However, there are only two in $I\bar{1}$: Ca(000) and Ca(z00). The Fourier difference map of $I\bar{1}$ anorthite (Angel et al. 1990; Ghose et al. 1993) shows a splitting of the Ca sites, which has been interpreted as a time or space average (Smith 1974; Angel et al. 1990; Ghose et al. 1993). The $I\bar{1}$ structure with unsplit sites only occurs at high pressure (Angel 1988). In other words, there is no $I\bar{1}$ structure model with single Ca sites for anorthites at ambient pressure.

Plagioclase with $I\bar{1}$ symmetry occurs on a nanometer scale (Figs. 3b and 3c) and, in distinction to the previous models, we interpret its structure as having Ca atoms that occupy a single site. Therefore, we generated a structure model with single Ca sites using the coordinates of an $I\bar{1}$ anorthite (Fig. 6a) (ICSD no. 86321, Angel et al. 1990) and doubled its unit cell along a. We obtained single sites by alternating ordered (o-i) and anti-ordered (i-o) arrays of Ca atoms (using the symbolism of Van Tendeloo et al. 1989), in which o indicates Ca(000) and Ca(z00) and i stands for Ca(0i0) and Ca(zi0) positions. This model (Fig. 6b) has an *I*-centered Si-Al framework and an ordered [where o-i represents Ca(000)-Ca(zi0)] and an anti-ordered [where i-o represents (Ca0i0)-Ca(z00)] Ca configuration along *a*. The model has $I\bar{1}$ symmetry and consists of two $P\bar{1}$ domains with displacement vector between them of R = 1/2[111]. The model is equivalent to that of the $I\bar{1}$ anorthite (ICSD no. 86321) if several ordered and anti-ordered cells are averaged.

HRTEM simulations

To examine the different degrees of transformation from $I\bar{1}$ to $P\bar{1}$ structures we performed HRTEM image simulations for one $I\bar{1}$ and two $P\bar{1}$ anorthites. Order parameters for these structures (An_{100}a, An_{100}b, and An_{100}c) are reported in Table 1.

HRTEM images were simulated for different values of sample thickness and defocus. Along the [1$\bar{1}$0] orientation only *a* and *c* reflections contribute to form an HRTEM image, and therefore we used this orientation to show the differences between the $I\bar{1}$ and $P\bar{1}$ structures. For each simulated structure we calculated

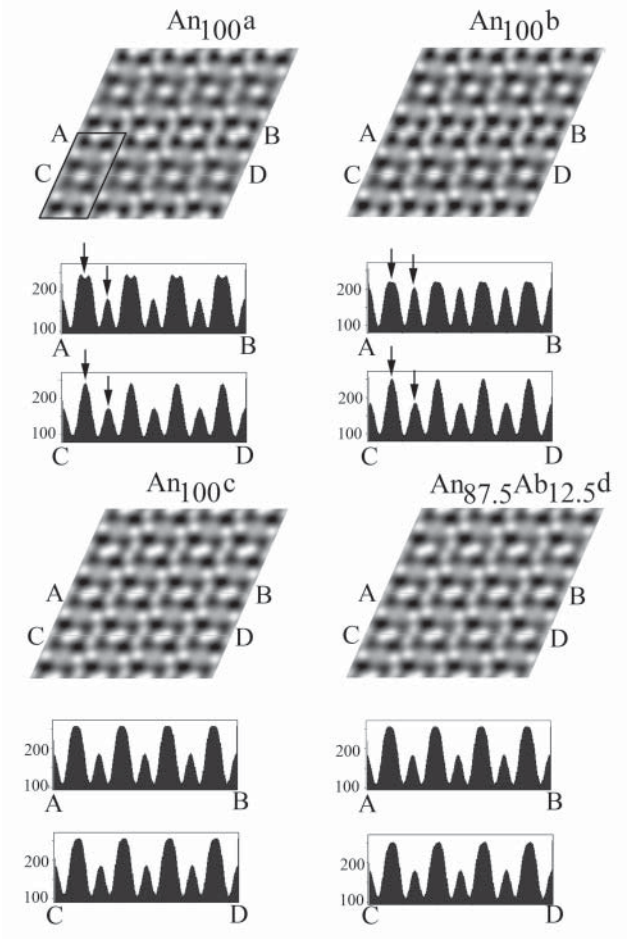

FIGURE 7. Simulated HRTEM images along [1$\bar{1}$0] of An_{100}a, An_{100}b, An_{100}c, and $An_{87.5}Ab_{12.5}$d structures at the microscope experimental conditions (defocus = –40 nm, sample thickness = 6.15 nm). Black lines border a unit cell. Intensity profiles of each image are calculated along lines AB and CD. The integrated areas are two pixels wide. Black arrows show intensity differences between traverses AB and CD in both An_{100}a and An_{100}b.

intensity profiles along AB and CD (Fig. 7). A unit cell is marked. The AB profile is along the cell edge, and CD is across the center of the cell. Significant differences exist in the intensities of the two profiles in both $P\bar{1}$ simulations (black arrows in the upper part of Fig. 7). As shown by the small vertical arrows, the difference is more pronounced in An_{100}a than in An_{100}b. As expected from the symmetry, in An_{100}c the intensities of the two traverses are identical. These HRTEM simulations prompt us to correlate the Q_d and structural changes with the intensity differences between the profiles along the cell edges and cell centers.

HRTEM image simulations were also performed to check possible effects of Na substitution for Ca. An anorthite unit cell contains eight anorthite formula units. Using two anorthite cells, two Ca atoms were exchanged for two Na atoms with an equivalent amount of Al for Si to obtain the $An_{87.5}Ab_{12.5}$ composition. These substitutions do not significantly affect the image ($An_{87.5}Ab_{12.5}$d in Fig. 7), indicating that such small changes in Ca content are not revealed in our HRTEM images.

TABLE 1. Symmetry and different order parameters for structure models used in the HRTEM simulations

	An_{100}a*	An_{100}b†	An_{100}c‡
Symmetry	$P\bar{1}$	$P\bar{1}$	$I\bar{1}$
Q_d	0.81§	Undetermined‖	0
Q_{od}	0.92#	0.78**	0.92#

* ICSD no. 86317 (Angel et al. 1990).
† ICSD no. 654 (Bruno et al. 1976).
‡ ICSD no. 86321 (Angel et al. 1990) with ordered and anti-ordered Ca configurations (details in $I\bar{1}$ anorthite section).
§ Calculated from the cell parameters in Angel et al. (1990) using the calibration of Redfern and Salje (1987).
‖ Intermediate between An_{100}a and An_{100}c.
Carpenter et al. (1990).
** Calculated from the structural data of Bruno et al. (1976).

Position-varying Q_d and structural differences in plagioclase

Simulated HRTEM images show that differences between intensity profiles of types AB (cell edge) and CD (cell center) can be used to detect the Q_d and structural differences for the $I\bar{1}$-$P\bar{1}$ transformation.

Here we use intensity profiles to follow symmetry and thus structural differences along the 00*l* fringes having either 1.28-nm or 0.64-nm periodicities (depending on whether they are in $P\bar{1}$ or $I\bar{1}$ domains) in adjacent areas of experimental HRTEM images. When considering adjacent areas on such small scales, we assume the experimental conditions (imaging conditions, orientations, and sample thickness) are constant. As intensity differences along the profiles are related to the $I\bar{1}$-$P\bar{1}$ transformation, such differences in experimental HRTEM images measured from place to place can be used to estimate Q_d and structural differences.

The intensity profile across the $P\bar{1}$ domains of the natural An_{100} sample shows no fluctuations (Fig. 8), which indicates that Q_d is uniform and the structure is unchanged across the imaged area. The intensity profiles across the HRTEM images of the synthetic An_{100} (Fig. 8), $An_{92}Ab_8$ (Fig. 9), and $An_{85}Ab_{15}$ (Fig. 9) are wavy. The synthetic An_{100} has the most pronounced waviness. Its intensity profile is non-periodic, and it has a definite minimum and maximum (black arrows in Fig. 8), which correspond to $P\bar{1}$ regions with the greatest deviation from $I\bar{1}$. A continuous gradation of intensity between the maximum and the minimum occurs through an intermediate that corresponds to a region of $I\bar{1}$ domain. The interpretation of the wavy intensity profile is that Q_d changes continuously from place to place, and structural differences occur in the synthetic An_{100} sample.

Differences along the corresponding intensity profiles also occur across the HRTEM images of $An_{92}Ab_8$ plagioclase (Fig. 9), but they are less pronounced than in synthetic An_{100}. In $An_{85}Ab_{15}$, slight intensity differences occur (Fig. 9), and these could represent incipient development of position-varying Q_d variations.

Structural fluctuations in plagioclase

The structure is unchanged and Q_d is uniform across the imaged region of the natural An_{100} sample. In contrast, continuous changes in Q_d from place to place and continuous structural differences, which we call structural fluctuations, occur in synthetic An_{100}, in $An_{92}Ab_8$, and in $An_{85}Ab_{15}$ samples.

Plagioclase with position-varying Q_d in closely spaced domains represents high strain energy and reduced surface energy

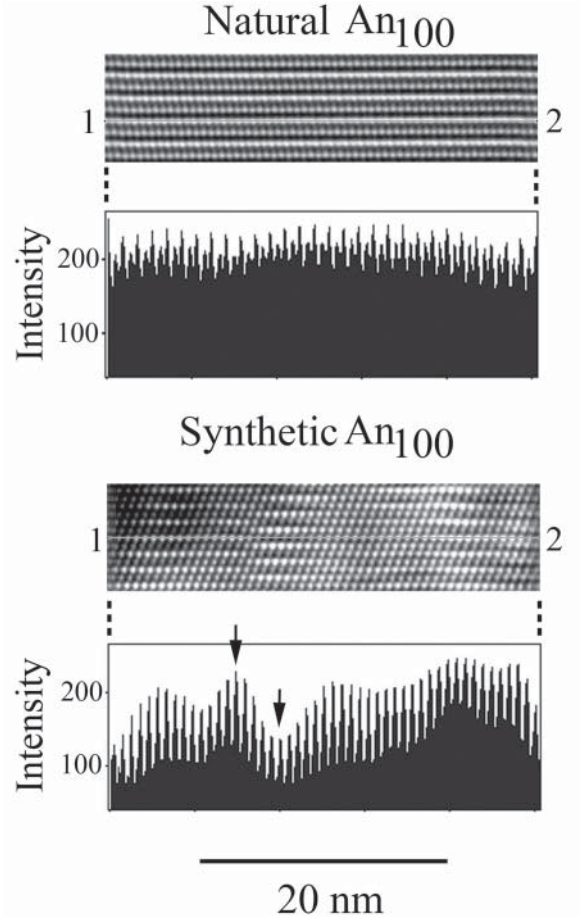

FIGURE 8. Background-filtered images of natural An_{100} along [010] (Fig. 2 between A and B) and synthetic An_{100} along [110] (Fig. 6 in Tribaudino et al. 2000), with their intensity profiles along the traverse between points 1 and 2 in the images. The integrated areas are two pixels wide. Black arrows in the synthetic An_{100} intensity profile show minimum and maximum intensities.

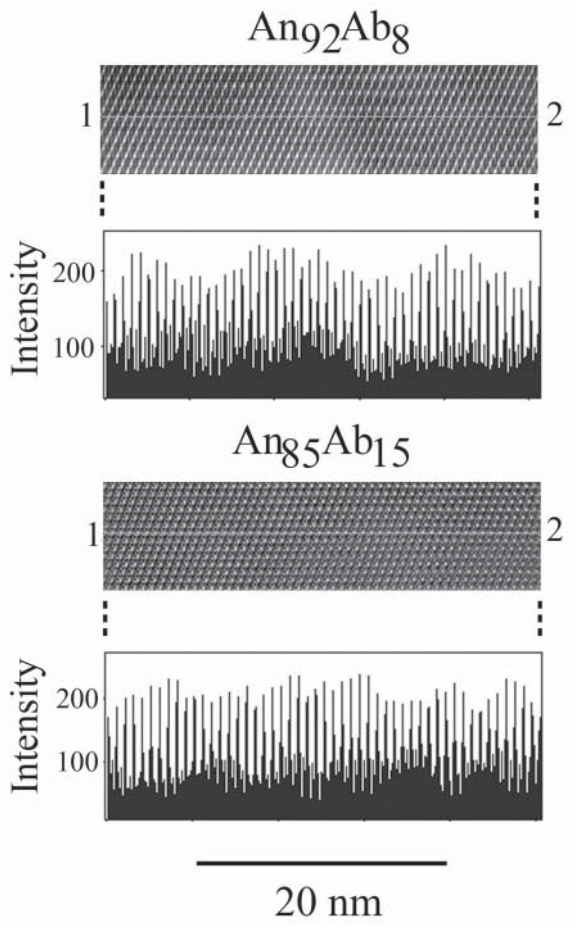

FIGURE 9. Background-filtered images of $An_{92}Ab_8$ along $[1\bar{1}0]$ (Fig. 3e between A and B) and $An_{85}Ab_{15}$ along [110] (Fig. 5c between A and B), with their intensity profiles along the traverse between points 1 and 2 in the images. The integrated areas are two pixels wide.

among the *c*-type domains (Salje 1992). Plagioclase crystals with uniform values of Q_d indicate low strain energy and high surface energy at the *c*-type boundary (Salje 1992). The IR spectra of plagioclase with large *c*-type domains differ from those with small *c*-type domains (Atkinson et al. 1999). Samples with large *c*-type domains correspond to plagioclases with uniform Q_d, and those with small *c*-type domains are plagioclases with different values of Q_d.

In natural An_{100}, the degree of Al-Si order is greater than in synthetic An_{100}, in $An_{92}Ab_8$, and in $An_{85}Ab_{15}$. Different order parameters of the investigated samples are reported in Table 2. The spontaneous strain, also called lattice strain, relating to the $I\bar{1}$-$P\bar{1}$ transition decreases with decreasing Al-Si order and Ca content (Redfern et al. 1988; Redfern 1992). We infer that decreasing Al-Si order and Ca content provides an explanation for the origin of the structural fluctuations in the synthetic An_{100}, $An_{92}Ab_8$, and $An_{85}Ab_{15}$ samples.

The structure is uniform within the $P\bar{1}$ domains in Al-Si ordered, homogeneous anorthite. In contrast, structural fluctuations develop in anorthites with decreasing Al-Si ordering, decreasing Ca content, or both. Such fluctuations are probably promoted by local inhomogeneities in ordering. The magnitudes of the fluctuations decrease with increases in Na content. In $An_{85}Ab_{15}$ plagioclase the fluctuations are present but weak, which may indicate some $P\bar{1}$ domains remain.

Uncertainties and ambiguities

Our HRTEM images of different Ca-rich plagioclase samples show evidence of structural fluctuations on the nanoscale. We observed such fluctuations in both anorthite with lower Al-Si ordering and in Na-bearing plagioclase. However, there is a potential ambiguity that needs consideration. The domain walls of the *c*-type domains are curvilinear (e.g., Van Tendeloo et al. 1989), and thus the domains are not constrained to having preferred orientations. It is therefore possible that superpositions of $I\bar{1}$ and $P\bar{1}$ domains can occur. Such superpositions can also occur if the domain sizes are comparable to the thickness of the foil (~10 nm). In these cases, overlap of the domains could result in

TABLE 2. Order parameters for the studied samples

	Natural An_{100}	Synthetic An_{100}	$An_{92}Ab_8$	$An_{85}Ab_{15}$
Q_d	uniform	position varying	position varying	position varying
Q_{od}	0.92*	0.85†	undetermined‡	0.85§

* Carpenter et al. (1990).
† Calculated from the cell parameters in Tribaudino et al. (2000).
‡ Carpenter et al. (1990) reported Q_{od} values between 0.85 and 0.88 in samples with similar composition and geological history.
§ Calculated from the structural data of Chiari et al. (1984).

variable values for Q_d. To resolve this potential ambiguity, one would need to tilt and obtain HRTEM images along different orientations of the same small area. Such experiments are extremely difficult. Challenges exist both in finding the same area at two or more different orientations and in recording the images at the same experimental conditions. Further complications arise since the experiments must be done rapidly to minimize sample degradation under the electron beam. The result is that, although we think we provide unique data about structural fluctuations on the nanoscale that reflect subtle variations in Al-Si ordering in Ca-rich plagioclase, further work is required to provide an unambiguous test of these results. The necessary techniques remain to be developed.

ACKNOWLEDGMENTS

Electron microscopy was completed at the John M. Cowley Center for High Resolution Electron Microscopy at Arizona State University. Financial support was provided by the Earth Sciences Division of the National Science Foundation via grant EAR-0440388. We thank M. Carpenter, M. Czank, and an anonymous reviewer for careful reviews. We are grateful to L.A.J. Garvie and David J. Smith for helpful discussions of the manuscript.

REFERENCES CITED

Angel, R.J. (1988) High-pressure structure of anorthite. American Mineralogist, 73, 1114–1119.
Angel, R.J., Carpenter, M.A., and Finger, L.W. (1990) Structural variation associated with compositional variation and order-disorder behavior in anorthite-rich feldspars. American Mineralogist, 75, 150–162.
Atkinson, A.J., Carpenter, M.A., and Salje, E.K.H. (1999) Hard mode infrared spectroscopy of plagioclase feldspars. European Journal of Mineralogy, 11, 7–21.
Brown, W.L. and Parsons, I. (1994) Feldspars in igneous rocks. In I. Parsons, Ed., Feldspars and their reactions, 421, p. 449–499. NATO ASI Series C: Mathematical and Physical Sciences, Kluwer, Dordrecht.
Brown, W.L., Hoffman, W., and Laves, F. (1963) Über kontinuierliche und reversibile Transformationen des Anorthits ($CaAl_2Si_2O_8$) zwischen 25 und 350 °C. Naturwissenschaften, 50, 221.
Bruno, E. and Facchinelli, A. (1979) Al-Si order-disorder and cell parameters in calcic plagioclases. Rendiconti Società Italiana di Mineralogia e Petrologia, 35, 59–69.
Bruno, E., Chiari, G., and Facchinelli, A. (1976) Anorthite quenched from 1530 °C. I. Structure refinement. Acta Crystallographica, B32, 3270–3280.
Carpenter, M.A. (1991) Mechanism and kinetics of Al-Si ordering in anorthite: I. Incommensurate structure and domain coarsening. American Mineralogist, 76, 1110–1119.
——— (1994) Subsolidus phase relations of the plagioclase feldspar solid solution. In I. Parsons, Ed., Feldspars and their reactions, 421, p. 221–269. NATO ASI Series C: Mathematical and Physical Sciences, Kluwer, Dordrecht.
——— (2006) Elastic properties of minerals and the influence of phase transitions. American Mineralogist, 91, 229–246.
Carpenter, M.A. and Salje, E.K.H. (1998) Elastic anomalies in minerals due to structural phase transitions. European Journal of Mineralogy, 10, 693–812.
Carpenter, M.A., McConnel, J.D.C., and Navrotsky, A. (1985) Enthalpies of ordering in the plagioclase feldspar solid solution. Geochimica et Cosmochimica Acta, 49, 947–966.
Carpenter, M.A., Angel, R.J., and Finger, L.W. (1990) Calibration of Al/Si order variations in anorthite. Contributions to Mineralogy and Petrology, 104, 471–480.
Chiari, G., Benna, P., and Bruno, E. (1984) The structure of bytownite (An_{85}). A new refinement. Zeitschrift für Kristallographie, 169, 35–49.
Czank, M., Landuyt, J.V., Schulz, H., Laves, F., and Amelinckx, S. (1973) Electron microscopy study of the structural changes as a function of temperature in anorthite. Zeitschrift für Kristallographie, 138, 403–418.
Dove, M.T. (1997) Theory of displacive phase transitions in minerals. American Mineralogist, 82, 213–244.
Ghose, S., McMullan, R.K., and Weber, H.P. (1993) Neutron diffraction studies of the $P\bar{1}$-$I\bar{1}$ transition in anorthite, $CaAl_2Si_2O_8$, and the crystal structure of the body-centred phase at 514 K. Zeitschrift für Kristallographie, 204, 215–237.
Kempster, C.J.E., Megaw, H.D., and Radoslovich, E.W. (1962) The structure of anorthite, $CaAl_2Si_2O_8$ I. Structure analysis. Acta Crystallographica, 15, 1005–1017.
Kono, Y., Ishikawa, M., and Arima, M. (2004) Discontinuous change in temperature derivative of Vp in lower crustal rocks. Geophysical Research Letters, 31, L22601, DOI: 10.1029/2004GL020964.
Kroll, H. and Ribbe, P.H. (1980) Determinative diagrams for Al, Si order in plagioclases. American Mineralogist, 65, 449–457.
Loewenstein, W. (1954) The distribution of Al in tetrahedra of silicates and aluminates. American Mineralogist, 39, 92–96.
McLaren, A.C. (1973) The domain structure of a transitional anorthite; a study by direct lattice-resolution electron microscopy. Contributions to Mineralogy and Petrology, 41, 47–52.
Meyer, C., Leber, M., and Krivanek, O. (1996) Digital Micrograph 2.5.7. Gatan Inc., Pleasanton, San Francisco.
Putnis, A. (1992) Introduction to Mineral Sciences. Cambridge University Press, U.K.
Redfern, S.A.T. (1992) The effect of Al/Si disorder on the $I\bar{1}$-$P\bar{1}$ co-elastic phase transition in Ca-rich plagioclase. Physics and Chemistry of Minerals, 19, 246–254.
Redfern, S.A.T. and Salje, E. (1987) Thermodynamics of plagioclase II: Temperature evolution of the spontaneous strain at the $I\bar{1}$-$P\bar{1}$ phase transition in anorthite. Physics and Chemistry of Minerals, 14, 189–195.
Redfern, S.A.T., Graeme-Barber, A., and Salje, E. (1988) Thermodynamics of plagioclase III: Spontaneous strain at the $I\bar{1}$-$P\bar{1}$ phase transition in Ca-rich plagioclase. Physics and Chemistry of Minerals, 16, 157–163.
Salje, E. (1987) Thermodynamics of plagioclase I: Theory of the phase transition in anorthite and Ca-rich plagioclase. Physics and Chemistry of Minerals, 14, 181–188.
Salje, E.K.H. (1992) Application of Landau theory for the analysis of phase transitions in minerals. Physics Reports, 215, 49–99.
Smith, J.V. (1974) Feldspar minerals, V. 1. Crystal structure and physical properties. Springer Verlag, Berlin.
Tribaudino, M., Benna, P., and Bruno, E. (2000) TEM observations on the $P\bar{1}$-$I\bar{1}$ phase transition in feldspars along the join $CaAl_2Si_2O_8$–$SrAl_2Si_2O_8$. American Mineralogist, 85, 963–970.
Van Tendeloo, G., Ghose, S., and Amelinckx, S. (1989) A dynamical model for the $P\bar{1}$-$I\bar{1}$ phase transition in anorthite, $CaAl_2Si_2O_8$ I. Evidence from Electron Microscopy. Physics and Chemistry of Minerals, 16, 311–319.

MANUSCRIPT RECEIVED NOVEMBER 11, 2006
MANUSCRIPT ACCEPTED FEBRUARY 22, 2007
MANUSCRIPT HANDLED BY JOSHUA FEINBERG